

# Superconductivity and phase stability of potassium-doped *p*-quinquephenyl

HPSTAR  
680-2019



Ge Huang<sup>a,1</sup>, Guo-Hua Zhong<sup>b,1</sup>, Ren-Shu Wang<sup>a,c</sup>, Jia-Xing Han<sup>d</sup>, Hai-Qing Lin<sup>d,\*</sup>,  
Xiao-Jia Chen<sup>a,\*\*</sup>

<sup>a</sup> Center for High Pressure Science and Technology Advanced Research, Shanghai, 201203, China

<sup>b</sup> Shenzhen Institutes of Advanced Technology, Chinese Academy of Sciences, Shenzhen, 518055, China

<sup>c</sup> School of Materials Science and Engineering, Hubei University, Wuhan, 430062, China

<sup>d</sup> Beijing Computational Science Research Center, Beijing, 100193, China

## ARTICLE INFO

### Article history:

Received 8 November 2018

Accepted 1 December 2018

Available online 3 December 2018

## ABSTRACT

The chain-like organic compounds with conjugated structure have the potential to become high temperature superconductors. Here, we show that *p*-quinquephenyl containing five phenyl rings connected in *para* position is superconducting when the compound is doped by potassium, with a critical temperature of 7.3K. The *dc* magnetic susceptibility measurements provide solid evidence for the presence of Meissner effect in potassium-doped *p*-quinquephenyl. The real part of the *ac* susceptibility shows exactly same transition temperature as that in *dc* magnetization, and the imaginary part of nearly zero value after transition implies the realization of zero-resistivity. The crystal structure prediction identifies the superconducting phase as  $K_3p$ -quinquephenyl with  $P2_1$  space-group, a layered structure. The occurrence of bipolarons revealed by Raman spectra guarantees potassium metal intercalated into *p*-quinquephenyl and suggests the important role of this elementary excitation played on superconductivity.

© 2018 Elsevier Ltd. All rights reserved.

## 1. Introduction

Organic superconductors provide abundant basis to understand fundamental properties of correlated electrons [1]. The large Coulomb correlation among conduction electrons, known as one of characterizations of organic superconductors, seems to be distinguished from the electron-phonon coupling in the conventional Bardeen-Cooper-Schrieffer (BCS) theory [2,3]. Furthermore, the critical temperatures ( $T_c$ 's) of these organic superconductors were predicted to be dramatically high because of high electron-electron interaction energy as discussed by V. L. Ginzburg and W. A. Little, respectively [4,5]. So far, superconductivity in these materials emerges with expense of some competing orders, such as charge density wave, spin density wave, antiferromagnetism, and so on [6,7]. The characteristic of these competing orders in the normal state of organic superconductors has been studied extensively

[8–11]. Organic metals were first observed to exhibit superconductivity in quasi-one-dimensional (TMTSF)<sub>2</sub>PF<sub>6</sub> by the use of pressure to overcome spin density wave order [8]. Antiferromagnetic order is also illustrated to compete with superconductivity in the  $\kappa$ -(BEDT-TTF)<sub>2</sub>X family ( $X = \text{Cu}[\text{N}(\text{CN})_2]\text{Cl}$ ,  $\text{Cu}[\text{N}(\text{CN})_2]\text{Br}$  and  $\text{Cu}(\text{NCS})_2$ ) [12] and the cubic alkali-metal doped fullerene C<sub>3</sub>C<sub>60</sub> [13]. Interestingly, the room temperature ferromagnetism was also observed in naphthalene [14].

In accordance to organic metals, conducting polymers, such as polyparaphenylene (PPP), possess low-dimensional nature and large Coulomb correlation. Polymer conductors also exhibit high electrical conductivities upon doping with donors or acceptors [15]. PPP is of chain-like structure with infinite benzene rings linked with C-C single bond. It shows typical nondegenerate ground-state property. Oligophenyls as models of PPP were found to undergo structure modification upon cooling by heat capacity measurement, X-ray diffraction (XRD), and Raman scattering measurement [16–18]. Comparing with original unit cell, the lattice constants are almost doubled in the *b* and *c* directions [19]. The softening phonon mode [18] in Raman spectra is exactly the same as the behaviors of the formation of charge-density-wave order in transition metal dichalcogenides, such as NbSe<sub>2</sub> [20–22]. The charge carriers in

\* Corresponding author.

\*\* Corresponding author.

E-mail addresses: [haiqing0@csrc.ac.cn](mailto:haiqing0@csrc.ac.cn) (H.-Q. Lin), [xjchen@hpstar.ac.cn](mailto:xjchen@hpstar.ac.cn) (X.-J. Chen).

<sup>1</sup> These authors contributed equally.

doped polymers are considered to be paramagnetic polarons ( $S = 1/2$ ) and diamagnetic bipolarons ( $S = 0$ ) with charge of  $-e$  (or  $+e$ ) and  $-2e$  (or  $+2e$ ). The electronic state and structural changes over several units are involved in the formation of polarons or bipolarons [23]. When dopants are taken into account, bipolarons are proved to be more stable excitation with negative effective correlation energy  $U_{eff}$ , the difference between the Coulomb repulsion and the lattice relaxation energy [24]. The characteristic of bipolarons is analogous to the Cooper pair in the BCS theory of superconductivity. All these features make conducting polymers as the promising candidates for high-temperature superconductors. Recently, *p*-terphenyl as a member of oligophenyls was pronounced to become superconductors upon doping potassium (K) metal with  $T_c$  at 7.2 K, 43 K and 123 K, respectively [25–27]. This chain-like *p*-terphenyl differs from the polycyclic aromatic hydrocarbons, such as phenanthrene [28,29], picene [30], coronene [31], and 1,2; 8,9-dibenzopentacene [32], due to the absence of zigzag and armchair edges. A superconducting phase with  $T_c$  as high as 107 K was reported in K-doped *p*-terphenyl flake as well [33]. Furthermore, the photoemission spectroscopy conducted in surface K-doped *p*-terphenyl crystals shows a gap persisting up to at least 120 K and shares similar temperature dependence with obtained spectra of Bi-Sr-Ca-Cu-O superconductors [34]. An analogous gap below 50 K was also found in K-doped *p*-terphenyl films fabricated on Au (111), the stubborn feature of this gap at the applied magnetic field up to 11 T indicates the high upper critical field for such a kind of high- $T_c$  superconductor [35]. Following these works, superconductivities in K-doped biphenyl [36] and triphenylbismuth [37] have also been reported.

Both the higher doping level and longer chain length are favor of huge increase of electrical conductivity for PPP [38]. We expect the existence of superconductivity in *p*-quinquephenyl ( $C_{30}H_{22}$ ) consisting of five benzene rings linked in the para position.  $C_{30}H_{22}$ , which can be seen as the most ideal, simple, rigid and symmetric molecule, has attracted increasing attention as liquid crystal [39,40]. Meanwhile,  $C_{30}H_{22}$  can be exploited in organic field-effect transistors because of its electrical properties [41]. In this work, we report the synthesis of the K-doped *p*-quinquephenyl ( $K_xC_{30}H_{22}$ ) and the observation of the Meissner effect in this material. Both *dc* and *ac* magnetic measurements support the existence of superconductivity in this material. Raman scattering measurements reveal the occurrence of bipolarons. Furthermore, we predict the crystal structure and the stability of this superconducting phase with help of the first-principles calculations. The observation of superconductivity in  $K_xC_{30}H_{22}$  adds a new member of oligophenyls superconductors after *p*-terphenyl.

## 2. Experiments

### 2.1. Material synthesis

K metal (99% purity) and  $C_{30}H_{22}$  (98% purity) were both purchased from Alfa Aesar. The synthesis method was reported earlier [25,36]. We got the black powder sample of  $K_xC_{30}H_{22}$  after sealing and annealing in quartz tube under high vacuum. The quartz tube was then heated to 380 °C in 70 min, and held at 340 °C for 3 days. The resulting black powder sample,  $K_xC_{30}H_{22}$  is completely different from the white pristine  $C_{30}H_{22}$ . K metal is easy to get oxidized when it is exposed to the air. All these experiments excluding annealing were done in glove box ( $O_2$  less than 0.1 ppm,  $H_2O$  less than 0.1 ppm).

### 2.2. Material characterization

The doped sample was sealed into nonmagnetic capsules for magnetization and Raman scattering measurements.

Magnetization measurements of both the *dc* and *ac* susceptibility were carried out on doped samples as functions of temperature and field by using a SQUID magnetometer (Quantum Design MPMS3). The temperature ranges from 1.8 K to 20 K and the external magnetic field was applied up to 1000 Oe. Raman spectroscopy measurements were performed on  $K_xC_{30}H_{22}$  and pristine  $C_{30}H_{22}$  in backscattering geometry by using an in-house system with Charge Coupled Device and Spectrometer from Princeton Instrument. The laser excitation was in a wavelength of 660 nm and power less than 1 mW to avoid damage to samples.

### 2.3. Theoretical calculations

To study the structural and electronic properties of  $K_xC_{30}H_{22}$ , we employed the Vienna *ab initio* simulation package (VASP) based on the projector-augmented wave method [42,43]. For the plane-wave basis-set expansion, an energy cutoff of 600 eV was adopted. The Monkhorst-Pack *k*-point grids are generated according to the specified *k*-point separation of  $0.02 \text{ \AA}^{-1}$ , and the convergence thresholds are set as  $10^{-6}$  eV in energy and  $10^{-3}$  eV/Å in force. The generalized gradient form (GGA) of the exchange-correlation functional (Perdew-Burke-Ernzerhof96) was adopted [44]. In addition, considering the nonlocal interaction, we have added the correction of van der Waals (vdW) in the version of vdW-DF2 in this calculation [45]. The necessity of vdW-DF2 functional has been confirmed by our previous studies [36,46–49].

## 3. Results and discussion

### 3.1. Meissner effect

The Meissner effect and zero resistivity are two fundamental features of superconductivity. Actually the metal-doped carbon-based superconductors were mainly detected from magnetic measurement [28,30–32]. However, with small diamagnetic volume and easily damaged crystal structure under pressure, the metallic state of  $K_xC_{30}H_{22}$  was hard to be realized even below  $T_c$ . Difficulties in detecting weak superconductivity from resistivity measurements can be overcome by using magnetic susceptibility experiments.

Fig. 1 shows the *dc* magnetic susceptibility  $\chi$  for the powder sample of  $K_xC_{30}H_{22}$  versus temperature measured in the

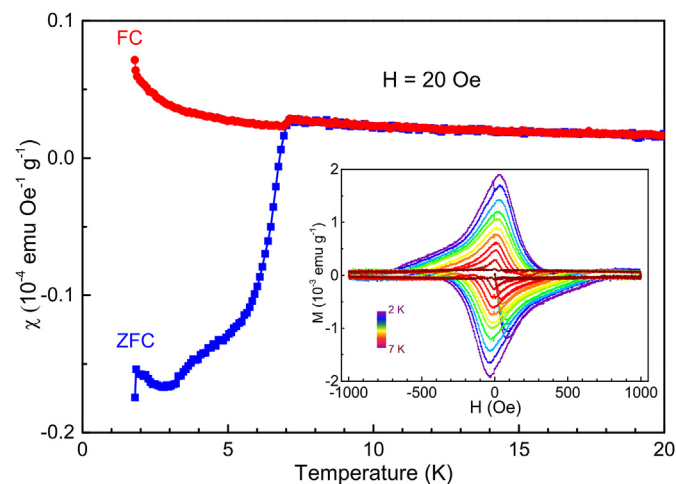


**Fig. 1.** Temperature dependence of the *dc* magnetic susceptibility for  $K_xp$ -quinquephenyl in a low magnetic field of 20 Oe, within the zero-field cooling and the field cooling cycles. Inset shows the magnetic hysteresis with applied field up to 1000 Oe at various temperatures below 7.3 K after the subtraction of the paramagnetic background. (A colour version of this figure can be viewed online.)

zero-field cooling (ZFC) and field cooling (FC) cycles at 20 Oe. It should be pointed out that the  $\chi$  in the ZFC run drops sharply below 7.3 K and then saturates. At around 5 K, the second step transition originates in the possibility for another superconducting phase. Meanwhile, the  $\chi$  in the FC run decreases slowly and the saturation value is much smaller, suggesting existence of pinning due to magnetic impurity. The temperature corresponding to the sharp drop is defined as  $T_c$ . The shielding fraction extracted from the ZFC  $\chi$  is only 0.074%, if we assume a density of about  $3 \text{ g cm}^{-3}$ . Such a small shielding fraction is due to the presence of the impurities of this powder sample. The diamagnetic signal is at least an order of magnitude smaller than the signal obtained in bulk sample [30,50]. Note that both ZFC and FC  $\chi$  show an upturn trend at a lower temperature than  $T_c$ , indicating the strong paramagnetic signal. The inset of Fig. 1 shows the  $M$  versus  $H$  plots obtained at different temperatures ranging from 2 K to 7 K with scanning field up to 1000 Oe after removing the paramagnetic backgrounds. The  $M(H)$  curves become totally nonlinear upon 100 Oe so that the lower critical field is close to 100 Oe. Nevertheless, the magnetization of  $\text{K}_x\text{C}_{30}\text{H}_{22}$  does not reach zero in applied fields up to 1000 Oe, implying the upper critical field is much higher than 1000 Oe. This diamond-like hysteresis loop is a typical character for the type-II superconductor.

Furthermore, we have also measured  $ac$  magnetic magnetization to confirm the existence of superconductivity in  $\text{K}_x\text{C}_{30}\text{H}_{22}$ . The complex  $ac$  magnetic susceptibility denoted as:  $\chi = \chi' + i\chi''$ , has been successfully used to determine some parameters of superconductivity, such as the critical temperature and magnetic fields, critical current density, London and Campbell penetration depths, the pinning potential, irreversibility line, and so on [51]. Fig. 2 shows the temperature dependence of the first harmonic  $ac$  magnetic susceptibility for  $\text{K}_x\text{C}_{30}\text{H}_{22}$  in an external  $ac$  magnetic field of 8 Oe and frequency at 234 Hz. The observation of double step-like transition in the real part of susceptibility  $\chi'$  can be ascribed to the screening properties and the granular nature of our samples [52]. The imaginary part of susceptibility  $\chi''$  exhibits a positive peak, indicating the penetration of the  $ac$  field into the sample. The  $T_c$  has been assigned to the separation point between  $\chi'$  and  $\chi''$ . After this point, the almost zero signal of  $\chi''$  upon cooling implies the realization of zero-resistivity in the superconductivity state [25,50,51].

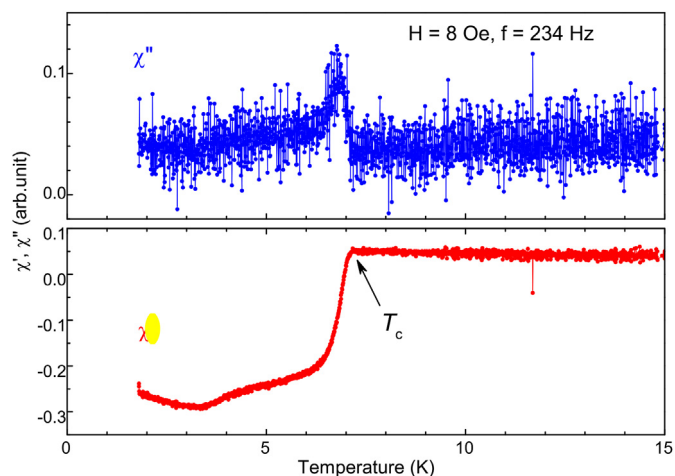


**Fig. 2.** Temperature dependence of the real ( $\chi'$ ) and imaginary ( $\chi''$ ) parts of the  $ac$  magnetic susceptibility of  $\text{K}_x\text{p}$ -quinquephenyl. (A colour version of this figure can be viewed online.)

Superconductivity in  $\text{K}_x\text{C}_{30}\text{H}_{22}$  has been detected by both the  $dc$  and  $ac$  magnetic measurements. The  $ac$  magnetic measurements have been widely used in cuprate and iron-based superconductors. However, the  $ac$  magnetic measurements are absent in most polycyclic aromatic hydrocarbon superconductors [53]. The resistivity measurements have been applied in organic salts to identify the superconducting phase, but the zero-resistivity in superconducting state was rarely achieved [7,54,55].

The magnetic field dependence of the magnetization for  $\text{K}_x\text{C}_{30}\text{H}_{22}$  at various temperatures with low applied fields is summarised in Fig. 3a. The linear behavior of magnetic-dependent magnetization signals the Meissner effect in this superconductor. The  $H_{c1}$  at selected temperatures is defined as the terminative point of transition from linear to nonlinear  $M(H)$  as shown in the smallest inset of Fig. 3a. The method used to determine  $H_{c2}$  is similar to the previous studies [56]. The regression coefficient  $R$  of a linear fit to the data points collected between 0 and  $H$ , is used as a function of  $H$ . The  $H_{c1}$  is determined based on the deviation from linear dependence of the  $R$  versus  $H$ . The lower critical fields  $H_{c1}$  at given temperatures are shown in the inset and the solid line represents the empirical law  $H_{c1}(T)/H_{c1}(0) = 1 - (T/T_c)^2$ . The lower critical field at zero-temperature  $H_{c1}(0)$  is  $24.2 \pm 0.6$  Oe.

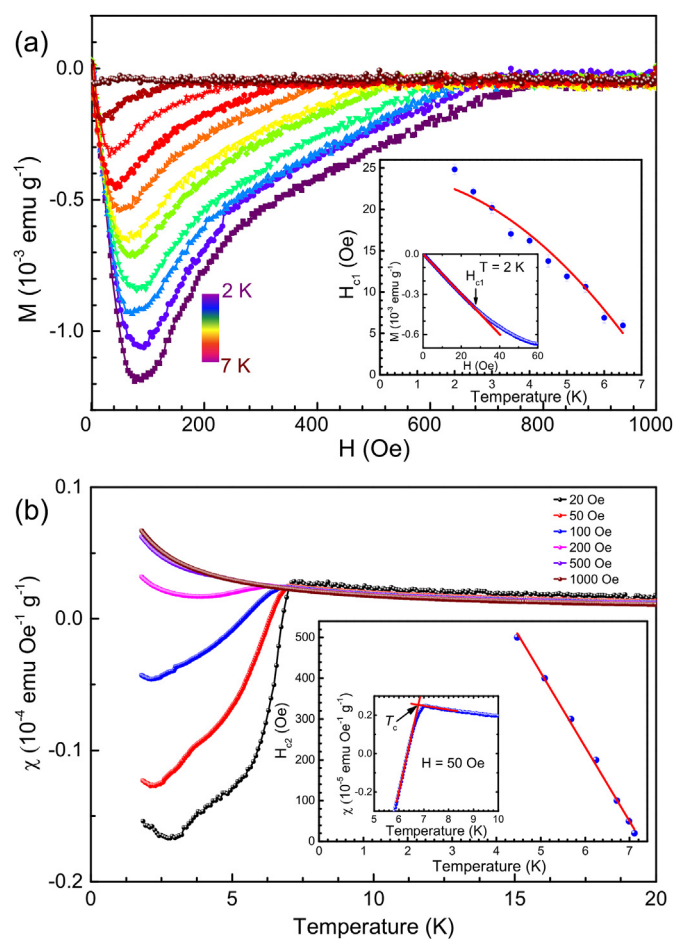


**Fig. 3.** (a) The initial part of  $M$ - $H$  curves measured at low fields at various temperature. Inset: The temperature dependence of lower critical field  $H_{c1}(T)$  and the determination of  $H_{c1}$  at temperature of 2 K given by the field dependent magnetization. (b) The temperature dependence of magnetic susceptibility for  $\text{K}_x\text{p}$ -quinquephenyl obtained at different magnetic fields in the zero-field cooling cycles. Inset: The temperature dependence of the upper critical field  $H_{c2}(T)$  and an example used to definite  $T_c$  by the magnetization versus temperature at the field of 50 Oe. (A colour version of this figure can be viewed online.)

Fig. 3b shows the temperature dependence of the magnetic susceptibility of our sample measured under applied fields in the ZFC run. The diamagnetic volume becomes smaller with increasing magnetic fields and  $T_c$  is thus decreased slowly towards lower temperature. It seems likely that the superconducting fraction is totally suppressed by applied field at 1000 Oe. However, due to the existence of strong paramagnetic impurities, the diamagnetic signal is covered by the strong background. The inset of Fig. 3b exhibits that the intercept of linear extrapolations from below and above superconducting transition is defined as  $T_c$ . As an example, the result measured at field of 50 Oe is shown. The upper critical field  $H_{c2}$  can not be definitely determined from these magnetic measurements [30]. The roughly estimation of  $H_{c2}$  as a function of temperature is shown in the inset of Fig. 3b. The straight line is the data fitting from the Werthamer-Helfand-Hohenberg formula [57]. We obtain the upper critical field at zero-temperature  $H_{c2}(0) = 1324.3 \pm 24.4$  Oe.

The zero-temperature superconducting London penetration depth  $\lambda_L$  and Ginzburg-Landau coherence length  $\xi_{GL}$  can be estimated from  $H_{c1}(0)$  and  $H_{c2}(0)$  by using the equations [58]:

$$H_{c2}(0) = \Phi_0 / 2\pi\xi_{GL}^2 \quad (1)$$

and

$$H_{c1}(0) = \left( \Phi_0 / 4\pi\lambda_L^2 \right) \ln(\lambda_L / \xi_{GL}), \quad (2)$$

where the quantum flux  $\Phi_0$  is  $2.0678 \times 10^{-15}$  Wb.  $\xi_{GL}$  of 498.6 Å and  $\lambda_L$  of 520.8 Å are obtained for this  $K_xC_{30}H_{22}$  superconductor from substituting  $H_{c1}(0)$  and  $H_{c2}(0)$ . The obtained Ginzburg-Landau parameter  $\kappa = \lambda_L / \xi_{GL} = 1.04$  also suggests that the  $K_xC_{30}H_{22}$  belongs to a type-II superconductor.

### 3.2. Raman spectra

Fig. 4 shows Raman spectra of  $C_{30}H_{22}$  and  $K_xC_{30}H_{22}$ . *p*-Quinquephenyl molecule has a benzenoid structure with five benzene rings aligned in para position, as shown in Fig. 4. All of these major peaks in pristine  $C_{30}H_{22}$  can be assigned and classified as five parts: rotational motion, ring deformation, ring breathing, C-H bending and C-C stretching [59,60]. The bipolaronic characterization in alkali-metal doped polyparaphenylenes synthesized by different method has been extensively studied in previous works [61,62]. The almost separated two intra-ring C-C stretching modes at around

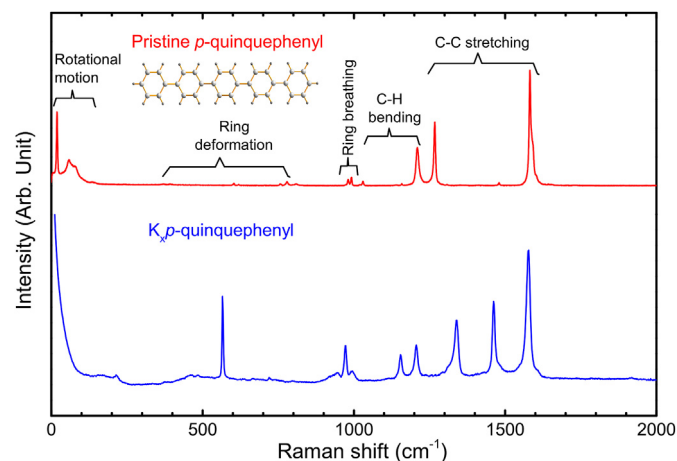


Fig. 4. Raman spectra of pristine *p*-quinquephenyl and  $K_x$ *p*-quinquephenyl measured at room temperature. (A colour version of this figure can be viewed online.)

1582  $cm^{-1}$  in parent sample downshift and merge to bipolaronic bands localized at 1576  $cm^{-1}$ . The observation of 1461  $cm^{-1}$  mode with no corresponding band in the pristine can be considered as the fingerprint for the formation of bipolarons. The band near 1268  $cm^{-1}$  assigned inter-ring C-C stretching upshifts to 1338  $cm^{-1}$  by intercalated K atoms into  $C_{30}H_{22}$ , indicating that the chain length becomes more coplanar [61]. The 1154  $cm^{-1}$  and 1206  $cm^{-1}$  modes presented in Raman spectra of doped samples are due to C-H external and internal stretching, respectively. These two peak are both evolved from 1211  $cm^{-1}$  mode in the pristine. The triple bands localized at 970  $cm^{-1}$  are from the formation of bipolarons. Raman characterization of  $K_xC_{30}H_{22}$  proves the existence of bipolarons, which possibly accounts for the observed superconductivity in K-doped *p*-terphenyl [25–27]. Recently, the quantum resonance between superconducting gaps near a Lifshitz transition has been proposed to be the driving mechanism for the observed superconductivity in these system [63].

### 3.3. Crystal structures and electronic properties

To identify this observed superconducting phase, we have investigated the crystal structures of  $K_xC_{30}H_{22}$  by using the first-principles calculations. The phase stability was studied by calculating the formation energy  $E_f$ . The calculation of the  $E_f$  for the doping level  $x$  is referred to previous studies [36,46–48]. Fig. 5 shows the formation energy of  $K_xC_{30}H_{22}$  ( $x = 1, 2, 3$  and 4) as a function of the K chemical potential.  $\mu_K$  is the chemical potential of the K specie and  $\mu_K(\text{bulk})$  can be obtained from the energy per K atom in the K metal with the *bcc* structure. Here  $\mu_K = \mu_K(\text{bulk})$  means that the element is so rich that the pure element phase can form.  $E_f < 0$  indicates that the doped compound is stably existent. As shown in Fig. 4,  $K_2C_{30}H_{22}$  is the most stable in a wide range chemical potential. However, under rich K condition,  $K_3C_{30}H_{22}$  becomes more stable. The result of thermodynamic stability indicates that both  $K_2C_{30}H_{22}$  and  $K_3C_{30}H_{22}$  can be easily fabricated in experiments.

Based on predicted crystal structures, we further compared the calculated XRD patterns with the experimental ones (crystal

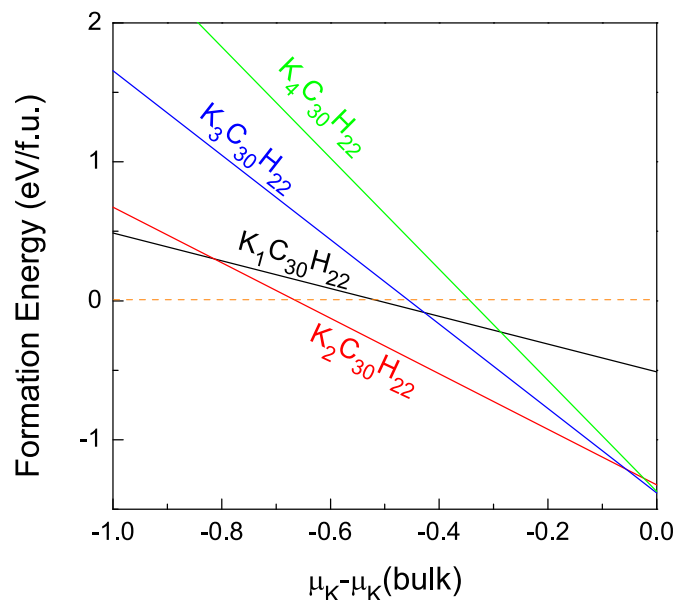
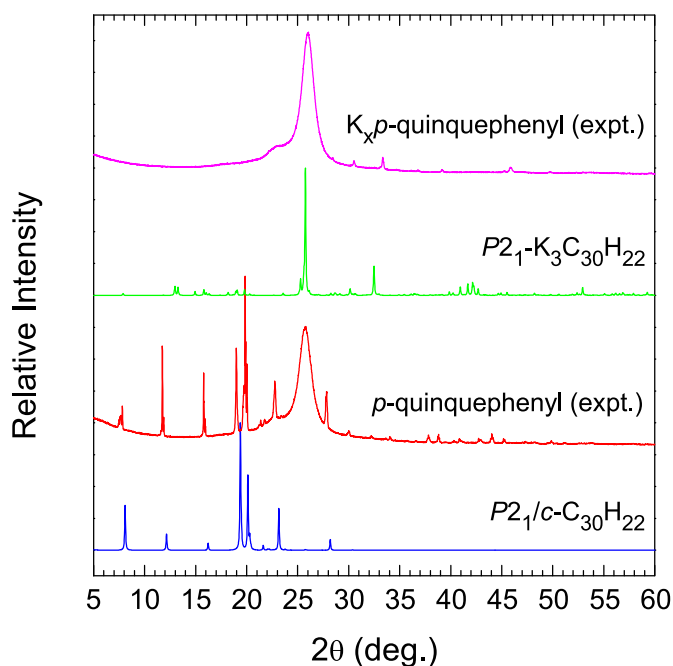


Fig. 5. Calculated formation energy of  $K_xC_{30}H_{22}$  as a function of the K chemical potential. (A colour version of this figure can be viewed online.)



**Fig. 6.** Calculated XRD spectra of pristine and doped *p*-quincephenyl.  $P2_1/c$ - $C_{30}H_{22}$  and  $P2_1$ - $K_3C_{30}H_{22}$  are corresponding to the theoretically predicted structures. The experimental XRD patterns were taken from the pristine and K-doped samples (the superconducting sample with  $T_c = 7.3$  K). All XRD data were collected by using the incident wavelength  $\lambda = 1.5406$  Å. (A colour version of this figure can be viewed online.)

structures and XRD spectra can be found in the [Supplementary material](#)) to determine the possible superconducting phase observed in our experiments. As shown in [Fig. 6](#), the XRD of the optimized structure of  $C_{30}H_{22}$  with the space-group of  $P2_1/c$  is in agreement with the experiment characterization. However, the phase transition occurs from  $P2_1/c$  to  $P2_1$  after doing. We found

that  $K_3C_{30}H_{22}$  with  $P2_1$  symmetry can produce the XRD patterns from the experiments. The XRD spectra of other structures are madly deviated from that of experimental sample (See the [Supplementary material](#)). Similar to K-doped biphenyl [36,64] and *p*-terphenyl [48,64], the results of the total energies at different magnetic states for  $K_xC_{30}H_{22}$  proved that  $K_2C_{30}H_{22}$ ,  $K_3C_{30}H_{22}$  and  $K_4C_{30}H_{22}$  are nonmagnetic while  $K_1C_{30}H_{22}$  is antiferromagnetic. Thus, the superconducting phase of 7.3 K is identified as  $P2_1$ - $K_3C_{30}H_{22}$ .

[Fig. 7a](#) shows the crystal configuration of  $P2_1$ - $K_3C_{30}H_{22}$ . A typical layered structure is observed and the organic molecule and K atom are almost coplanar. All of K atoms are over the C-C bonds viewing along the *a* direction. The optimized lattice parameters are  $a = 6.914$  Å,  $b = 22.619$  Å,  $c = 6.981$  Å and  $\gamma = 82.2^\circ$ , respectively. The volume of the doped system is expanded 12.8% than the pristine *p*-quincephenyl. The charge of about 2.2 e/f.u. transfers from K atoms to organic molecules which results in the metallization of *p*-quincephenyl. As shown in [Fig. 7b](#),  $P2_1$ - $K_3C_{30}H_{22}$  exhibits the metallic feature with two bands crossing the Fermi level. The electronic density of states (DOS) at Fermi level is about 4.9 states/eV/f.u., which is close to that of two-electron-doped benzene [65]. Low DOS value at Fermi level is a possible reason for such a low  $T_c$  of 7.3 K. In other words, higher  $T_c$  can be obtained by tuning the electronic states at Fermi level. Both changing the doping level and pressure are the feasible approaches [46,66].

#### 4. Conclusions

We have investigated the K-doped *p*-quincephenyl combining experimental with theoretical methods. The superconductivity with  $T_c \sim 7.3$  K in  $K_xC_{30}H_{22}$  is proved by both the *dc* and *ac* magnetic measurements. The magnetic magnetization at various temperatures and fields reveals the Meissner effect in the superconducting state. The Ginzburg-Landau parameter  $\kappa = 1.04$  suggests that  $K_xC_{30}H_{22}$  is a type-II superconductor. The bipolaronic band characteristic was observed from Raman spectra. Based on the analysis on stability and XRD, theoretical calculations identified the

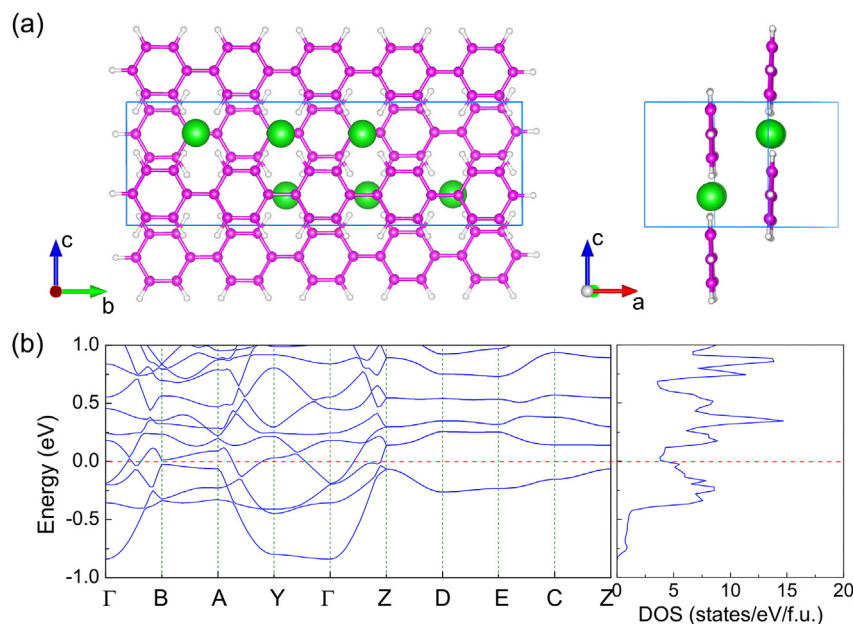


**Fig. 7.** (a) Optimized crystal structure of  $P2_1$ - $K_3C_{30}H_{22}$  viewing from different directions. Green balls represent K atoms. (b) Calculated electronic band structures along high-symmetrical *k*-point path and density of states (DOS).  $\Gamma(0,0,0)$ , B(0.5,0,0), A(0.5,0,0), Y(0.0,0.5), Z(0,0,0.5), D(0.5,0,0.5), E(0.5,0.5,0.5) and C(0,0.5,0.5). Zero energy denotes the Fermi level. (A colour version of this figure can be viewed online.)

superconducting phase as  $P2_1-K_3C_{30}H_{22}$  with the layered structure. The K doping results in the transitions of crystal structure and electronic properties.  $P2_1-K_3C_{30}H_{22}$  exhibits the metallic behavior due to the charge transferring from K atoms to quinquephenyl molecules. We thus have discovered a new member of oligophenyls superconductors, which is significant for exploring the high temperature superconductors and understanding the superconductivity in organic materials.

## Acknowledgments

Experiments were supported by the National Key R&D Program of China (Grant No. 2018YFA0305900). The calculations were supported by the National Natural Science Foundation of China (Grant Nos. 61574157 and 61774164), the Basic Research Program of Shenzhen (Grant Nos. JCYJ20170818153404696 and JCYJ20150925163313898), and NSAF U1530401. The partial calculations were supported by the Special Program for Applied Research on Super Computation of the NSFC-Guangdong Joint Fund (the second phase) under Grant No. U1501501.

## Appendix A. Supplementary data

Supplementary data to this article can be found online at <https://doi.org/10.1016/j.carbon.2018.12.001>.

## References

- [1] O. Gunnarsson, Superconductivity in fullerides, *Rev. Mod. Phys.* 69 (1997) 575–606.
- [2] J. Bardeen, L.N. Cooper, J.R. Schrieffer, Theory of superconductivity, *Phys. Rev.* 108 (1957) 1175–1204.
- [3] J. Bardeen, L.N. Cooper, J.R. Schrieffer, Microscopic theory of superconductivity, *Phys. Rev.* 106 (1957) 162–164.
- [4] W.A. Little, Possibility of synthesizing an organic superconductor, *Phys. Rev.* 134 (1964) A1416–A1424.
- [5] V.L. Ginzburg, On surface superconductivity, *Phys. Lett.* 13 (1964) 101–102.
- [6] M. Capone, M. Fabrizio, C. Castellani, E. Tosatti, Colloquium: modeling the unconventional superconducting properties of expanded  $A_3C_{60}$  fullerides, *Rev. Mod. Phys.* 81 (2009) 943–958.
- [7] A. Ardavan, S. Brown, S. Kagoshima, K. Kanoda, K. Kuroki, H. Mori, et al., Recent topics of organic superconductors, *J. Phys. Soc. Jpn.* 81 (2012), 011004.
- [8] D. Jerome, A. Mazaud, M. Ribault, K. Bechgaard, Superconductivity in a synthetic organic conductor (TMTSF) $_2$ PF $_6$ , *J. Phys. Lett.* 41 (1980) L95–L98.
- [9] S. Lefebvre, P. Wzietek, S. Brown, C. Bourbonnais, D. Jérôme, C. Mézière, et al., Mott transition, antiferromagnetism, and unconventional superconductivity in layered organic superconductors, *Phys. Rev. Lett.* 85 (2000) 5420.
- [10] D.S. Chow, F. Zamborszky, B. Alavi, D.J. Tantillo, A. Baur, C.A. Merlic, et al., Charge ordering in the TMTTF family of molecular conductors, *Phys. Rev. Lett.* 85 (2000) 1698.
- [11] P. Monceau, F.Y. Nad, S. Brazovskii, Ferroelectric Mott-Hubbard phase of organic (TMTTF) $_2$ X conductors, *Phys. Rev. Lett.* 86 (2001) 4080.
- [12] R.H. McKenzie, Similarities between organic and cuprate superconductors, *Science* 278 (1997) 820–821.
- [13] Y. Takabayashi, A.Y. Ganin, P. Jeglic, D. Arcon, T. Takano, Y. Iwasa, et al., The disorder-free non-BCS superconductor  $Cs_3C_{60}$  emerges from an antiferromagnetic insulator parent state, *Science* 323 (2009) 1585–1590.
- [14] X.-L. Wu, R.-S. Wang, J. Cheng, G.-H. Zhong, X.-J. Chen, Y. Gao, et al., Room temperature ferromagnetism in naphthalene, *Carbon* 136 (2018) 125–129.
- [15] M. Dubois, D. Billaud, Solid state electrochemical intercalation of lithium and sodium ions into polyparaphenylene, *J. Solid State Chem.* 127 (1996) 123.
- [16] J.L. Baudour, Y. Delugeard, H. Cailleau, Transition structurale dans les polyphényles. I. Structure cristalline de la phase basse température du *p*-terphényle à 113 K, *Acta Crystallogr. Sect. B Struct. Crystallogr. Cryst. Chem.* 32 (1976) 150–154.
- [17] S.S. Chang, Heat capacity and thermodynamic properties of *p*-terphenyl: study of order-disorder transition by automated high-resolution adiabatic calorimetry, *J. Chem. Phys.* 79 (1983) 6229.
- [18] A. Girard, H. Cailleau, Y. Marqueton, C. Ecolivet, Raman scattering study of the order-disorder phase transition in *para*-terphenyl, *Chem. Phys. Lett.* 54 (1978) 479–482.
- [19] K.N. Baker, A.V. Fratini, T. Resch, H.C. Knachel, W.W. Adams, E.P. Socci, et al., Crystal structures, phase transitions and energy calculations of poly (*p*-phenylene) oligomers, *Polymer* 34 (1993) 1571–1587.
- [20] X.X. Xi, L. Zhao, Z.F. Wang, H. Berger, L. Forró, J. Shan, et al., Strongly enhanced charge-density-wave order in monolayer NbSe $_2$ , *Nat. Nanotechnol.* 10 (2015) 765–769.
- [21] S.S. Wang, J.M. Chen, Raman spectrum of metallic layered compound NbSe $_2$ , *Solid State Commun.* 14 (1974) 1145–1148.
- [22] X.T. Zhu, Y.W. Cao, J.D. Zhang, E.W. Plummer, J.D. Guo, Classification of charge density waves based on their nature, *Proc. Natl. Acad. Sci. U. S. A.* 112 (2015) 2367–2371.
- [23] K. Honda, Y. Furukawa, K. Furuya, H. Torii, M. Tasumi, Density functional theory study on the Raman spectra of negative polarons and negative bipolarons in Na-doped poly(*p*-phenylene), *J. Phys. Chem. A* 106 (2002) 3587–3592.
- [24] P.A. Lane, X. Wei, Z.V. Vardeny, Studies of charged excitations in  $\pi$ -conjugated oligomers and polymers by optical modulation, *Phys. Rev. Lett.* 77 (1996) 1544.
- [25] R.-S. Wang, Y. Gao, Z.-B. Huang, X.-J. Chen, Superconductivity in *P*-Terphenyl, 2017 arXiv:1703.05803.
- [26] R.-S. Wang, Y. Gao, Z.-B. Huang, X.-J. Chen, Superconductivity at 43 K in a Single C-C Bond Linked Terphenyl, 2017 arXiv: 1703.05804.
- [27] R.-S. Wang, Y. Gao, Z.-B. Huang, X.-J. Chen, Superconductivity above 120 Kelvin in a Chain Link Molecule, 2017 arXiv: 1703.06641.
- [28] X.F. Wang, R.H. Liu, Z. Gui, Y.L. Xie, Y.J. Yan, J.J. Ying, et al., Superconductivity at 5 K in alkali-metal-doped phenanthrene, *Nat. Commun.* 2 (2011) 507.
- [29] Q.-W. Huang, G.-H. Zhong, J. Zhang, X.-M. Zhao, C. Zhang, H.-Q. Lin, X.-J. Chen, Constraint on the potassium content for the superconductivity of potassium-intercalated phenanthrene, *J. Chem. Phys.* 140 (2013) 114301.
- [30] R. Mitsuhashi, Y. Suzuki, Y. Yamanari, H. Mitamura, T. Kambe, N. Ikeda, et al., Superconductivity in alkali-metal-doped picene, *Nature* 464 (2010) 76–79.
- [31] Y. Kubozono, H. Mitamura, X. Lee, X. He, Y. Yamanari, Y. Takahashi, et al., Metal-intercalated aromatic hydrocarbons: a new class of carbon-based superconductors, *Phys. Chem. Chem. Phys.* 13 (2011) 16476–16493.
- [32] M.Q. Xue, T.B. Cao, D.M. Wang, Y. Wu, H.X. Yang, X.L. Dong, et al., Superconductivity above 30 K in alkali-metal-doped hydrocarbon, *Sci. Rep.* 2 (2012) 389.
- [33] P. Neha, V. Sahu, S. Patnaik, Facile Synthesis of Potassium Intercalated *P*-terphenyl and Signatures of a Possible High  $T_c$  Phase, 2017 arXiv:1712.01766.
- [34] H.X. Li, X.Q. Zhou, S. Parham, T. Nummy, J. Griffith, K. Gordon, et al., Spectroscopic Evidence of Low Energy Gaps Persisting towards 120 Kelvin in Surface-doped *P*-terphenyl Crystals, 2017 arXiv:1704.04230.
- [35] M.Q. Ren, W. Chen, Q. Liu, C. Chen, Y.J. Qiao, Y.J. Chen, et al., Observation of Novel Gapped Phases in Potassium Doped Single Layer *P*-terphenyl on Au, vol 111, 2017 arXiv:1705.09901.
- [36] G.-H. Zhong, D.-Y. Yang, K. Zhang, R.-S. Wang, C. Zhang, H.-Q. Lin, et al., Superconductivity and phase stability of potassium-doped biphenyl, *Phys. Chem. Chem. Phys.* 20 (2018) 25217–25223.
- [37] R.-S. Wang, J. Cheng, X.-L. Wu, H. Yang, X.-J. Chen, Y. Gao, Z.-B. Huang, Superconductivity at 3.5 K and/or 7.2 K in potassium-doped triphenylbismuth, *J. Chem. Phys.* 149 (2018) 144502.
- [38] E.E. Havinga, L.W. Van Horssen, Dependence of the electrical conductivity of heavily-doped poly-*p*-phenylenes on the chain length, *Synth. Met.* 16 (1986) 55–70.
- [39] Y. Olivier, L. Muccioli, C. Zannoni, Quinquephenyl: the Simplest rigid-rod-like nematic liquid crystal, or is it? An atomistic simulation, *ChemPhysChem* 15 (2014) 1345–1355.
- [40] T.J. Dingemans, N.S. Murthy, E.T. Samulski, Javelin-, hockey stick-, and boomerang-shaped liquid crystals, Structural variations on *p*-quinquephenyl, *J. Phys. Chem. B* 105 (2001) 8845–8860.
- [41] D.J. Gundlach, Y.Y. Lin, T.N. Jackson, D.G. Schlom, Oligophenyl-based organic thin film transistors, *Appl. Phys. Lett.* 71 (1997) 3853.
- [42] G. Kresse, J. Furthmüller, Efficiency of *abinitio* total energy calculations for metals and semiconductors using a plane-wave basis set, *Comput. Mater. Sci.* 6 (1996) 15–50.
- [43] G. Kresse, J. Furthmüller, Efficient iterative schemes for *abinitio* total-energy calculations using a plane-wave basis set, *Phys. Rev. B* 54 (1996) 11169–11186.
- [44] J.P. Perdew, K. Burke, M. Ernzerhof, Generalized gradient approximation made simple, *Phys. Rev. Lett.* 77 (1996) 3865.
- [45] K. Lee, É.D. Murray, L. Kong, B.I. Lundqvist, D.C. Langreth, Higher-accuracy van der Waals density functional, *Phys. Rev. B* 82 (2010), 081101(R).
- [46] G.-H. Zhong, C. Zhang, X.W. Yan, X.G. Li, Z. Du, G.X. Jing, et al., Structural and electronic properties of potassium doped 1,2;8,9-Dibenzopentacene superconductor: comparing with doped [7]-Phenacenes, *Mol. Phys.* 115 (2017) 472–483.
- [47] X.H. Wang, G.H. Zhong, X.W. Yan, X.J. Chen, H.Q. Lin, First-principles prediction on geometrical and electronic properties of K-doped chrysene, *J. Phys. Chem. Solids* 104 (2017) 56–61.
- [48] G.-H. Zhong, X.-H. Wang, R.-S. Wang, J.-X. Han, C. Zhang, X.-J. Chen, et al., Structural and bonding characteristics of potassium-doped *p*-terphenyl superconductors, *J. Phys. Chem. C* 122 (2018) 3801–3808.
- [49] X.-W. Yan, C. Zhang, G.H. Zhong, D.W. Ma, M. Gao, The atomic structures and electronic properties of potassium-doped phenanthrene from a first-principles study, *J. Mater. Chem. C* 4 (2016) 11566.
- [50] R.A. Hein, Ac magnetic susceptibility, Meissner effect, and bulk superconductivity, *Phys. Rev. B* 33 (1986) 7539.
- [51] F. Gomory, Characterization of high-temperature superconductors by ac susceptibility measurements, *Supercond. Sci. Technol.* 10 (1997) 523–542.
- [52] M. Polichetti, M.G. Adesso, D. Zola, J.L. Luo, G.F. Chen, Z. Li, et al., Granularity

- and vortex dynamics in LaFeAsO<sub>0.92</sub>Fo<sub>0.08</sub> probed by harmonics of the *ac* magnetic susceptibility, Phys. Rev. B 78 (2008) 224523.
- [53] Y. Kubozono, R. Eguchi, H. Goto, S. Hamao, T. Kambe, T. Terao, et al., Recent progress on carbon-based superconductors, J. Phys.-Condes. Matter 28 (2016) 334001.
- [54] K. Teranishi, X. He, Y. Sakai, M. Izumi, H. Goto, R. Eguchi, et al., Observation of zero resistivity in K-doped picene, Phys. Rev. B 87 (2013), 060505.
- [55] H. Taniguchi, M. Miyashita, K. Uchiyama, K. Satoh, N. Mori, H. Okamoto, et al., Superconductivity at 14.2 K in layered organics under extreme pressure, J. Phys. Soc. Jpn. 72 (3) (2003) 468–471.
- [56] M. Abdel-Hafez, P.J. Pereira, S.A. Kuzmichev, T.E. Kuzmicheva, V.M. Pudalov, L. Harnagea, et al., Lower critical field and SNS-Andreev spectroscopy of 122-arsenides: evidence of nodeless superconducting gap, Phys. Rev. B 90 (2014), 054524.
- [57] N.R. Werthamer, E. Helfand, P.C. Hohenberg, Temperature and purity dependence of the superconducting critical field, *H<sub>c2</sub>*. III. Electron spin and spin-orbit effects, Phys. Rev. 147 (1966) 295.
- [58] M. Tinkham, Introduction to Superconductivity, McGraw-Hill, New York, 1975.
- [59] K. Honda, Y. Furukawa, Conformational analysis of *p*-terphenyl by vibrational spectroscopy and density functional theory calculations, J. Mol. Struct. 735–736 (2005) 11–19.
- [60] H. Ohtsuka, Y. Furukawa, M. Tasumi, Dependencies of the Raman spectra of *p*-oligophenyls on the chain length and the excitation wavelength, Spectroc. Acta Pt. A-Molec. Spectr. 49 (1993) 731–737.
- [61] M. Dubois, G. Froyer, G. Louarn, D. Billaud, Raman spectroelectrochemical study of sodium intercalation into poly(*p*-phenylene), Spectroc. Acta Pt. A-Molec. Biomolec. Spectr. 59 (2003) 1849–1856.
- [62] Y. Furukawa, H. Ohtsuka, M. Tasumi, Raman studies of polarons and bipolarons in sodium-doped poly-*p*-phenylene, Synth. Met. 55 (1993) 516–523.
- [63] M.V. Mazziotti, A. Valletta, G. Campi, D. Innocenti, A. Perali, and Antonio Bianconi, Possible Fano resonance for high-*T<sub>c</sub>* multi-gap superconductivity in *p*-terphenyl doped by K at the Lifshitz transition, Europhys. Lett. 118 (2017) 37003.
- [64] G.-H. Zhong, C. Zhang, M. Chen, X.-J. Chen, H.-Q. Lin, Magnetic transitions in K-doped biphenyl and *p*-terphenyl, IEEE Trans. Magn. 54 (2018) 7002105.
- [65] G.-H. Zhong, X.-J. Chen, H.-Q. Lin, Prediction of Superconductivity in Potassium-doped Benzene, 2015 arXiv:1501.00240.
- [66] G.-H. Zhong, C.-L. Yang, X.-J. Chen, H.-Q. Lin, Superconductivity in solid benzene molecular crystal, J. Phys.-Condes. Matter 30 (2018) 245703.